Multi-scale MAP Despeckling of SONAR Images

A. Isar and D. Isar
Electronics and Telecommunications Faculty, "Politehnica" University Timisoara, Romania
alexandru.isar@etc.utt.ro

S. Moga
Ecole Nationale Supérieure des Télécommunications de Bretagne
Brest, France
sorin.moga@enst-bretagne.fr

J.-M. Augustin and X. Lurton
IFREMER, Centre de Brest
Service Acoustique et Sismique (TMSI/AS),
France
Jean.Marie.Augustin@ifremer.fr

***Abstract* - The SONAR images are perturbed by a multiplicative noise called speckle, due to the coherent nature of the scattering phenomenon. The use of speckle reduction filters is necessary to optimize the images exploitation procedures. This paper presents a new speckle reduction method in the wavelets domain using a novel Bayesian-based algorithm, which tends to reduce the speckle, preserving the structural features (like the discontinuities) and textural information of the scene. A blind speckle-suppression method that performs a non-linear operation on the data, based on a new bishrink filter variant is obtained. Finally, some simulation examples prove the performances of the proposed denoising method. These performances are compared with the results obtained applying state-of-the-art speckle reduction techniques.**

I. INTRODUCTION

The SONAR systems exploits techniques developed in the radar field and the capabilities of the high resolution imagery in a great number of applications such: marine geology, commercial fishing, offshore oil prospecting and drilling, cable and pipeline laying and maintenance and underwater warfare, [1]. The SONAR images represent a particular case of SAR images. Some classical estimators, used to denoise SAR images are, [2]:
- the Kuan filter (least mean square error linear estimator),
- the Frost filter (Wiener filter adapted to multiplicative noise).

Between the modern estimators can be found:
- the marginal MAP filter (for the maximization of the a posteriori probability), [3],
- the multiresolution MAP filter (a combination between a marginal MAP filter and a multiscale transform), [4].

A new estimators category uses the wavelets theory, [3], [4], [5], [6]. The corresponding denoising methods have three steps:
1) the computation of the forward wavelet transform, WT,
2) the filtering of the result obtained,
3) the computation of the inverse wavelet transform of the result obtained, IWT.

Some comparisons between the application of the classical speckle reduction filters and the application of the denoising methods based on wavelets, in the case of SAR images, were proved the superiority of this last category of methods, [6-7]. Numerous WTs can be used to operate these treatments. The first wavelet transform used in denoising applications was the Discrete Wavelet Transform, DWT. This transform is most commonly used in its maximally decimated form (Mallat's dyadic filter tree), [8-9]. It has three main disadvantages, [10]: lack of shift invariance, lack of symmetry of the mother wavelets and poor directional selectivity. The first disadvantage can be reduced using the Cycle Spinning, [11]. The second disadvantage can be eliminated using complex WT, [12] or biorthogonal WT, [13]. But in the last case the orthogonality is lost. Unfortunately, the influence of the third disadvantage can not be reduced. In the following, the Dual Tree Complex Wavelet Transform, DT CWT, [10,14], will be used. This is a redundant WT, with a redundancy of 4. Its architecture is based on two trees, each implementing a DWT, [15]. All the WTs have two parameters: the mother wavelets, MW and the primary resolution, PR, (number of iterations). The importance of their selection is highlighted in [16]. Numerous filter types can be used in the WT domain: the Wiener filter, [17], that minimizes the mean square estimation error, the hard-thresholding filter, [18], that realizes a very simple treatment, the soft-thresholding filter, [18, 7, 4], that minimizes the Min-Max estimation error, the marginal MAP filter, [3], or the bishrink filter, [14]. Some variants of those filters were used in [4,5,7]. In [3] and [6] two special types of MAP filters were used. Unfortunately, these filters have not closed-form input-output relations. Their application requires the use of numerical methods. This paper proposes a new denoising method for SONAR images based on the combination of the DT CWT with a variant of the bishrink filter. This variant has a closed-form input-output relation. The second section presents the architecture of the proposed denosing system and the third section establishes a statistical analysis of the proposed denoising method. The aim of the forth section is the presentation of some simulation results. These performances are compared with the results of state-of-the-art speckle reduction techniques.

II. THE DENOISING METHOD

The SONAR images are perturbed by a multiplicative noise of speckle type,

$$i_r(\tau_1,\tau_2) = i_o(\tau_1,\tau_2)\cdot n_r(\tau_1,\tau_2). \quad (2.1)$$

The hypothesis of the independence of the random processes i_0 and n_r, can be adopted, when the speckle is fully developed, [3,6]. The architecture of the denoising system proposed is presented in fig. 1.

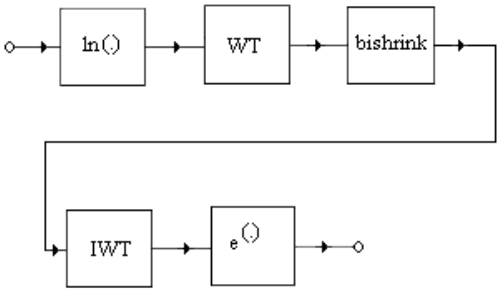

Fig. 1. The architecture of the denoising system.

The WT is applied after the transformation of the multiplicative noise into an additive one. The coefficients of this transform are filtered using the variants of the bishrink filter, proposed in this paper. At the system output, after the computation of the IWT, the logarithm inversion and the mean compensation, the estimation of the useful image, $\hat{i}_0(\tau_1,\tau_2)$, is measured.

III. A STATISTICAL ANALYSIS OF THE DENOISING SYSTEM

This analysis will be done block after block, following Fig. 1.

A. The input image

The speckle perturbing a SONAR image is a white noise with the energy distributed following a law χ^2:

$$f_{\chi^2}(a) = e^{-a} \quad \text{for} \quad a \geq 0. \tag{3.1}$$

The useful part of the input image has a similarly distribution, [1]. This model is a particularization of the model of SAR images, that is a Gamma distribution. The mean and the variance of the speckle noise equal 1.

B. The image at the output of the logarithm computation system

The first block, in fig. 1, transforms the initial probability density function, pdf, into a pdf of $\log-\chi^2$ type:

$$f_{\log-\chi^2}(a) = e^a \cdot e^{-e^a}, \tag{3.2}$$

with the mean and the variance given by the following relations, [19] :

$$\mu_{\log-\chi^2} = -\gamma, \tag{3.3}$$

where γ is the Euler's number and:

$$\sigma^2_{\log-\chi^2} = \frac{\pi^2}{6}. \tag{3.4}$$

Because the mean in (3.3) is not unitary, the logarithm computation procedure requires a mean correction, [6]. This correction can be realized at the end of the proposed denoising method. The mean of i_r is equal with the mean of i_o. The mean of i_r is estimated before the computation of the logarithm. This value is used after the inversion of the logarithm. The mean of the result obtained is substracted from this result and the mean of i_r is added. So, the mean of the obtained estimation, $\hat{i}_o$, will be equal with the mean of i_o. Taking into account the strong connection between the DT CWT and the DWT, already described, in the following, a statistical analysis of the DT CWT trough a correspondent analysis of the DWT is presented.

C. The DWT statistical analysis

At every DWT's iteration, the lines of the input image (obtained at the end of the previous iteration) are low-pass filtered with a filter having the impulse response m_0 and high-pass filtered with the filter with the impulse response m_1. Then the lines of the two images obtained at the output of the two filters are decimated with a factor of 2. Next the columns of the two images obtained are low-pass filtered with m_0 and high-pass filtered with m_1. The columns of those four images are also decimated with a factor of 2. Four new images (representing the result of the current iteration) are obtained. The first one, obtained after two low-pass filtering is named approximation image (or LL image). The others three are named detail images: LH, HL and HH. The LL image represents the input for the next iteration. In the following the coefficients of the DWT will be noted with ${}_xD_m^k$, where *x* represents the image who's DWT is computed, *m* represents the iteration index and *k=1*, for the HH image, *k=2*, for the HL image, *k=3*, for the LH image and *k=4*, for the LL image. These coefficients are computed using the following relation:

$${}_xD_m^k[n,p] = \left\langle x(\tau_1,\tau_2), \psi^k_{m,n,p}(\tau_1,\tau_2) \right\rangle, \tag{3.5}$$

where the wavelets can be factorized:

$$\psi^k_{m,n,p}(\tau_1,\tau_2) = \alpha^k_{m,n,p}(\tau_1) \cdot \beta^k_{m,n,p}(\tau_2), \tag{3.6}$$

and the two factors can be computed using the scale function $\varphi(\tau)$ and the mother wavelets $\psi(\tau)$ with the aid of the following relations:

$$\alpha^k_{m,n,p}(\tau) = \begin{cases} \varphi_{m,n}(\tau), & k = 1,4 \\ \psi_{m,n}(\tau), & k = 2,3 \end{cases}$$
$$\beta^k_{m,n,p}(\tau) = \begin{cases} \varphi_{m,n}(\tau), & k = 2,4 \\ \psi_{m,n}(\tau), & k = 1,3 \end{cases} \tag{3.7}$$

where:

$$\varphi_{m,n}(\tau) = 2^{-\frac{m}{2}} \varphi\left(2^{-m}\tau - n\right);$$
$$\psi_{m,n}(\tau) = 2^{-\frac{m}{2}} \psi\left(2^{-m}\tau - n\right). \tag{3.8}$$

1) The pdf of the wavelet coefficients

The pdf of the wavelet coefficients, ${}_xD_m^k$, can be expressed with the aid of the pdf of the input image, *x*, using the relation, [3]:

$$f_{x D_m^k}(a) = \underset{q_1=1}{\overset{M(k)}{*}} \underset{r_1=1}{\overset{N(k)}{*}} \underset{q_2=1}{\overset{M_0}{*}} \underset{r_2=1}{\overset{M_0}{*}} \ldots \underset{q_m=1}{\overset{M_0}{*}} \underset{r_m=1}{\overset{M_0}{*}} f_d(k, q_1, r_1, \ldots, q_m, r_m, a), \tag{3.9}$$

where:

$$f_d(k, q_1, r_1, \ldots, q_m, r_m, a) = G(k, q_1, r_1, \ldots, q_m, r_m) \cdot f_x\left(G(k, q_1, r_1, \ldots, q_m, r_m)\, a\right), \tag{3.10}$$

and :

$$G(k, q_1, r_1, \ldots, q_m, r_m) = \frac{1}{F(k, q_1, r_1) \prod_{l=2}^{m} m_0[q_l]\, m_0[r_l]}, \tag{3.11}$$

where :

$$F(k, q_1, r_1) = \begin{cases} m_0[q_1]\, m_0[r_1] & \text{for} \quad k = 4 \\ m_0[q_1]\, m_1[r_1] & \text{for} \quad k = 3 \\ m_1[q_1]\, m_0[r_1] & \text{for} \quad k = 2 \\ m_1[q_1]\, m_1[r_1] & \text{for} \quad k = 1 \end{cases}, \tag{3.12}$$

M_0 represents the length of the impulse response m_0, M_1 the length of m_1 and the numbers of the first two groups of convolutions in relation (3.9) are given by the relation (3.13).

In conformity with (3.9), the pdf of the wavelet coefficients is a sequence of convolutions. Hence, the random variable representing the wavelet coefficients can be written like a sum of independent random variables. So, the central limit theorem can be applied. This is the reason why the pdf of the wavelet coefficients tends asymptotically to a Gaussian, when the number of all convolutions in (3.9) tends to infinity. This number depends on the mother wavelets used and on the number of iterations of the DWT.

$$M(k) = \begin{cases} M_0 & \text{for} \quad k = 4 \\ M_0 & \text{for} \quad k = 3 \\ M_1 & \text{for} \quad k = 2 \\ M_1 & \text{for} \quad k = 1 \end{cases}$$

and (3.13)

$$N(k) = \begin{cases} M_0 & \text{for} \quad k = 4 \\ M_1 & \text{for} \quad k = 3 \\ M_0 & \text{for} \quad k = 2 \\ M_1 & \text{for} \quad k = 1 \end{cases}$$

For mother wavelets with a long support, this number becomes high very fast (for a small number of iterations). The mother wavelet with the shortest support is the Haar mother wavelets. In its case, the most difficult for this analysis, the relation (3.9) can be particularized in the form (3.14), after the first iteration. In fig. 2 are represented the pdfs of the wavelet coefficients obtained after the second iteration of the DWT of an image with a $\log-\chi^2$ pdf. Gaussians are also represented with dotted lines.

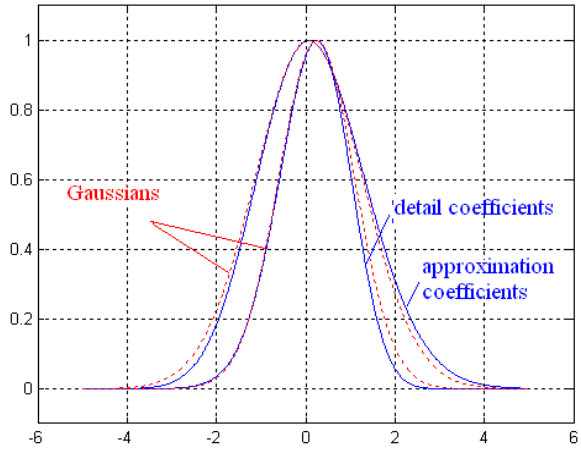

Fig. 2. The normalized pdfs of the wavelet coefficients obtained using Haar mother wavelets.

$$f_{x D_m^k}(c) = \begin{cases} 16\left(f_x(d) * f_x(d) * f_x(d) * f_x(d)\right), \\ k = 4 \\ 16\left(f_x(-d) * f_x(d) * f_x(-d) * f_x(d)\right), \\ k = 1,2,3 \end{cases} \tag{3.14}$$

$$d = 2c,$$

Because the difference between the pdfs of the wavelet coefficients obtained after the second iteration and the Gaussian is small, and because the support of the mother wavelets used in practice is longer than the support of the Haar mother wavelets, used in this example, we conclude that after two iterations the pdfs of the wavelet coefficients can be considered Gaussians.

For the first two iterations, heavy-tailed models must be considered. Finer analysis, measuring the distance between the real pdfs and Gaussians, are performed in [3], [6] and [19].

2) *The correlation of the wavelet coefficients*

The input image, *x*, represents the sum of the logarithm of the useful image, *s*, and of the logarithm of the speckle image, *n*. Because these two random signals are not correlated, the correlation of the wavelet coefficients of the image *x*, can be written in the following form:

$$\Gamma_{x D_m^k} = \Gamma_{s D_m^k} + \Gamma_{n D_m^k}. \tag{3.15}$$

The correlation function of the wavelet coefficients can be computed using the following relation:

$$\Gamma_{x D_m^k}[n_1, n_2, p_1, p_2] = \frac{1}{4\pi^2} \cdot \int_{\mathbb{R}^2} \gamma_x\left(2^{-m}\upsilon_1, 2^{-m}\upsilon_2\right) \cdot \left|\Im_2\left\{\psi^k(\upsilon_1, \upsilon_2)\right\}\right|^2 e^{-j\left[\upsilon_1(n_2-n_1)+\upsilon_2(p_2-p_1)\right]} d\upsilon_1 d\upsilon_2, \tag{3.16}$$

where $\gamma(x)$ represents the power spectral density of the random signal *x* and $\Im_2$ represents the two dimensional Fourier transform operator. Taking into account the fact that the input noise is white, with a variance $\pi^2/6$, it

can be written:

$$\gamma_n\left(2^{-m}\upsilon_1, 2^{-m}\upsilon_2\right)=\frac{\pi^2}{6}, \tag{3.17}$$

and the expression of the wavelet coefficients of the input noise image correlation function becomes:

$$\Gamma_{{}_nD_m^k}[n_1,p_1]=\frac{\pi^2}{6}\cdot\delta[n_1]\cdot\delta[p_1]. \tag{3.18}$$

So, the wavelet coefficients sequences of the noise component of the input image are white noise images having the same variance. The first and second order moments of the wavelet coefficients can be computed using the following relations:

$$E\left\{{}_xD_m^k[n_1,p_1]\right\}= =\begin{cases}0, & k=1,2,3\\ 2^m\cdot\mu_x, & k=4.\end{cases} \tag{3.19}$$

Only the means of the images formed with the approximation wavelet coefficients are not nulls. The following relation gives the mean of the DWT of the noise component of the input image:

$$E\left\{{}_nD_m^k[n_1,p_1]\right\}=\begin{cases}0, & k=1,2,3\\ -2^m\gamma, & k=4\end{cases}. \tag{3.20}$$

The DWT of the input noise component, n, has a variance given by:

$$\sigma^2_{{}_nD_m^k}=\begin{cases}\dfrac{\pi^2}{6}, & k=1,2,3\\ \dfrac{\pi^2}{6}-2^{2m}\gamma^2 & k=4.\end{cases} \tag{3.21}$$

The correlation of the DWT of s is given by:

$$\Gamma_{{}_sD_m^k}[n_1,p_1]=2^{2m}\cdot\Gamma_s\left[2^m n_1, 2^m p_1\right], \tag{3.22}$$

its mean by:

$$E\left\{{}_sD_m^k[n_1,p_1]\right\}=\begin{cases}0, & k=1,2,3\\ 2^m\cdot\mu_s, & k=4,\end{cases} \tag{3.23}$$

and its variance, by:

$$\sigma^2_{{}_sD_m^k}=2^{2m}\cdot\sigma_s^2. \tag{3.24}$$

So, the variance of the detail wavelet coefficients sequences, obtained starting from the useful component of the input image, increases when the iteration index increases.

D. The bishrink filter

Let ${}^1x$ be the considered detail coefficient and ${}^2x$ its parent (the detail coefficient at the same position but at the following iteration). In fact for a given parent corresponds a zone composed by four child coefficients. This is the reason why every image containing parent coefficients will be over sampled to have the same number of pixels like the corresponding image formed with child coefficients. The statistical parameters of the child coefficients (mean, variance), will be estimated using the parent coefficients having the same position and the neighbor child coefficients, located in a rectangular window, centered on the current child coefficient. It can be written:

$${}^1x={}^1s+{}^1n, \tag{3.25}$$

and:

$${}^2x={}^2s+{}^2n, \tag{3.26}$$

or, with vectorial notations:

$$\boldsymbol{x}=\boldsymbol{s}+\boldsymbol{n}. \tag{3.27}$$

The MAP estimation of $\boldsymbol{s}$, realized using the observation $\boldsymbol{x}$, is given by, [14]:

$$\hat{\boldsymbol{s}}(\boldsymbol{x})=\arg\max_{\boldsymbol{s}}\left\{\ln\left(\mathrm{p}_{\boldsymbol{n}}(\boldsymbol{x}-\boldsymbol{s})\cdot\mathrm{p}_{\boldsymbol{s}}(\boldsymbol{s})\right)\right\}. \tag{3.28}$$

Tacking into account the considerations already made, in the following we will consider that the DT CWT of the noise component is distributed following a Gaussian with a null mean, [3,5,6], the model of the first two iterations of the DT CWT of the useful image will be a Laplace distribution, [14], and for the other iterations this model will be Gaussian.

The noise variance estimation can be done using the relation, [21]:

$$\hat{\sigma}_n^2=\frac{median\left(\left|x[n_1,p_1]\right|\right)}{0.6475}\quad (n_1,p_1)\in HH. \tag{3.29}$$

The useful component DT CWT variance must be estimated locally. In this estimation process the correlation between the values of the same wavelet coefficient computed at two successive scales can be exploited. For this purpose the following relations can be used. First the local mean of the DT CWT of the useful component must be estimated:

$$\mu_{({}^bs)}[n_1,p_1]=\frac{1}{(2P+1)^2}\cdot\sum_{(n_2,p_2)\in{}^bW_{n_1,p_1}}{}^bx[n_2,p_2] \tag{3.30}$$

where $b=1$ or 2.

Then, the variance of the DT CWT of the input image, contained in the moving window ${}^bW_{n_1,p_1}$, can be computed:

$${}^b\hat{\sigma}_x^2[n_1,p_1]=\frac{1}{(2P+1)^2}\sum_{(n_2,p_2)\in{}^bW_{n_1,p_1}}\left({}^bx[n_2,p_2]-\mu_{({}^sb)}[n_2,p_2]\right)^2 \tag{3.31}$$

Using these values, the useful component DT CWT variance is given by:

$${}^b\hat{\sigma}^2[n_1,p_1]=\max\left(0,\ {}^b\hat{\sigma}_x^2[n_1,p_1]-\hat{\sigma}_n^2\right) \tag{3.32}$$

But, applying the relation (3.24), a theoretical result of this paper, a different estimation of the local variance of the child coefficients can be obtained:

$${}^1\hat{\sigma}_d=\frac{{}^2\hat{\sigma}}{2} \tag{3.33}$$

To profit of these two estimations of the useful component DT CWT local variances, obtained at two

successive scales, it can be written:

$$\hat{\hat{\sigma}}^{1} = \frac{\hat{\sigma}^{1} + \frac{\hat{\sigma}^{2}}{2}}{2} \tag{3.34}$$

and the input-output relations of the two variants of the bishrink filter that will be used in the following becomes:

$$\hat{s}^{1} = \frac{\left(\sqrt{\left({}^{1}x\right)^{2} + \left({}^{2}x\right)^{2}} - \frac{\sqrt{3}\hat{\sigma}_{n}^{2}}{\hat{\hat{\sigma}}^{1}}\right)_{+}}{\sqrt{\left({}^{1}x\right)^{2} + \left({}^{2}x\right)^{2}}} \cdot {}^{1}x, \tag{3.35}$$

for the first two iterations of the DT CWT and:

$$\hat{s}^{1} = \frac{\hat{\hat{\sigma}}^{1} \cdot \hat{\sigma}^{2}}{\hat{\hat{\sigma}}^{1} \cdot \hat{\sigma}^{2} + \hat{\sigma}_{n}^{2}} \cdot {}^{1}x \tag{3.36}$$

for the following iterations.

IV. SIMULATION RESULTS

A comparison between the results of different speckle reduction methods is presented in the following table. The image Lena was perturbed with a multiplicative Rayleigh noise, obtaining the input image. This image was treated using: a running averager, a median filter, the Lee's filter, the Kuan's filter, the Gamma filter, the Frost's filter and the proposed denoising method. The mean square errors obtained after the treatments are presented in table I.

The first parameter of each filter represents its window size. The second represents, the so-called, filter's parameter. These quantities were selected to minimize the mean square error of the result for the considered image. All the parameters of the proposed denoising method are selected automatically. Finally, a real image was treated. The original SONAR image is presented in fig. 3. It can be seen that the speckle is fully developed. The result obtained, using the proposed denoising method, is presented in fig. 4.

Analyzing the two images it can be observed that the noise was practically entirely removed and the fact that the details of the useful part of the input image (textures or edges) were not affected by the treatment proposed. An objective measure of the performances of a denoising method for SONAR images is the enhancement of the equivalent number of looks, ENL. This is a measure of the performances obtained in homogenous zones. The ENL is defined with the following relation:

$$\mathrm{ENL} = \left(\frac{\text{mean}}{\text{standard deviation}}\right)^{2}. \tag{4.1}$$

Considering the same homogenous region in fig. 3 and 4, the input ENL value (computed in figure 3) is of 7.34 and the output ENL value (computed in fig. 4) is of 76.64. The result from fig. 4 was obtained computing four iterations of the DT CWT. This value represents a superior bound of the iterations number for an image

TABLE I
A COMPARISON OF SEVEN SPECKLE REDUCTION METHODS

Noisy Image	3635
Averager 5	571.7
Median 7	569.8
Lee 7-5	807.5
Kuan 9-5.5	732.8
Gamma 5-1.5	595.5
Frost 5-1	566
Proposed	372.7

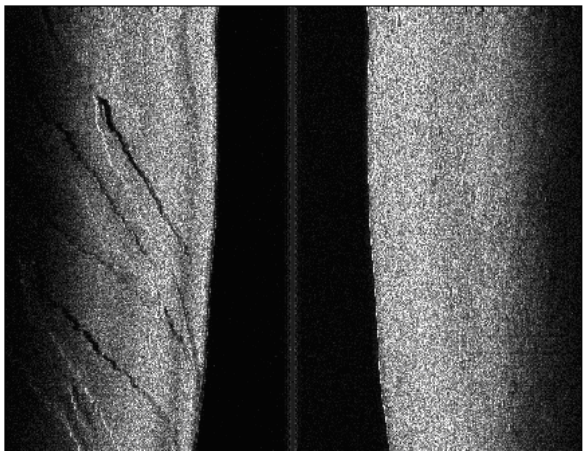

Fig.3. The input image.

Fig. 4. The result obtained.

with 1024x1024 pixels when the bishrink filter is used, taking into account the estimations described by the relations (3.30)-(3.32). For a higher iterations number the quality of those approximations decreases. The good quality of the image from fig. 4 proves the validity of the theoretical results presented.

V. CONCLUSION

A new denosing method for the processing of SONAR images was proposed. It is based on the use of the DT CWT and of two original variants of bishrink filter. This method combines image multiscale analysis and classical techniques of adaptive filtering. It permits to retain coefficients produced by significant structures present in the useful part of the input image and suppress those

produced by the speckle noise. A complete statistical analysis of this method was reported. Its hypotheses and results were confirmed by simulations. From $\log-\chi^2$ assumptions for the pdf of the reflectivity and the speckle we have expressed the pdf of the wavelet coefficients. For the first two iterations of the DT CWT, those pdfs corresponds to heavy-tailed distributions. We have approximated those distributions with a Laplace pdf. For the following iterations these pdf can be considered Gaussians. Using these hypotheses a MAP filter with closed-form input output relation was derived. Its parameters are locally estimated. In this estimation process a very important property of the WTs, the correlation between wavelet coefficients at the same position and successive scales, is exploited.

Because two different estimations of the local variance of the child wavelet details of the useful component of the input image are at our disposal, they are combined to increase the precision of this estimation. An adaptive mean correction method was also proposed. We evaluated the results on both synthetic data and real SONAR images, validating the theoretical hypotheses used. Further improvements could be obtained if a better WT and a 3D bishrink filter would be used. The latter avenue is currently under investigation and results will be reported soon.

ACKNOWLEDGMENTS

The research with the results reported in this paper was realized in the framework of the Programme de recherche franco-roumain Brancusi with the title: Débruitage des images SONAR en utilisant la théorie des ondelettes : applications aux systèmes d'aide à la décision pour la classification.

REFERENCES

[1] Laureant Hellequin, Jean-Marc Boucher, Xavier Lurton, "Processing of High-Frequency Multibeam Echo Sounder for Seafloor Characterization", *IEEE Journal of Oceanic Engineering*, vol. 28, no.1, pp. 78-89, January 2000.

[2] Roger Fjortoft, Armand Lopés, Frédéric Adragna, "Radiometric and Spatial Aspects of Speckle Filtering", *Proc. IGARSS'2000*, Honolulu, Hawaii, 24-28 July 2000.

[3] Samuel Foucher, Gozé Bertin Bénié, Jean-Marc Boucher, "Multiscale MAP Filtering of SAR images", *IEEE Transactions on Image Processing*, vol. 10, no.1, pp. 49-60, January 2001.

[4] Langis Gagnon, "Wavelet Filtering of Speckle Noise-Some Numerical Results", *Proceedings of the conference Vision Interface*, Trois Riviers, Canada, 1999.

[5] A. Pizurica, W. Philips, I. Lemahieu, M. Acheroy, "A Wavelet Based Image Denoising Technique Using Spatial Priors", *Proc ICIP 2000*, pp. 296-299, Vancouver, Sep. 2000.

[6] Alin Achim, Panagiotis Tsakalides and Anastasios Bezerianos, "SAR Image Denoising via Bayesian Wavelet Shrinkage Based on Heavy-Tailed Modeling", *IEEE Transactions on Geoscience and Remote Sensing*, Vol. 41, No. 8, pp. 1773-1784, August 2003.

[7] L. Gagnon, A. Jouan," Speckle Filtering of SAR Images-A Comparative Study Between Complex Wavelet-Based and Standard Filters", *Proc. of SPIE #3169 Conference* "Wavelet Applications in Signal and Image Processing V", San Diego, 1997.

[8] S. G. Mallat, "A Theory for Multiresolution Signal Decomposition: The Wavelet Representation" *IEEE Trans. PAMI*, 11, pp. 674-693, 1989.

[9] I. Daubechies, Ten Lectures on Wavelets, CBMS-NSF *Reg. Conf. Series in Appl. Math., SIAM*, Philadelphia, PA. 1992.

[10] N. Kingsbury, "Complex Wavelets for Shift Invariant Analysis and Filtering of Signals", *Applied and Computational Harmonic Analysis* 10, pp. 234-253, 2001.

[11] R. R. Coifman and D. L. Donoho, "Translation-Invariant Denoising", in *Wavelets and Statistics*, A. Antoniadis and G. Oppenheim Eds., Springer-Verlag, New York, 1995, 125-150.

[12] J. M. Lina, L. Gagnon, "Image enhancements with symmetric Daubechies' wavelets", Wavelet Applications in Signal and Image Processing III, *Proc. SPIE #2569*, pp. 196-207, 1995.

[13] Albert Cohen and Ingrid Daubechies, "A stability criterion for biorthogonal wavelet bases and their related subband coding schemes", *Duke Math. J.*, 68, pp. 313-335, 1992.

[14] L. Sendur and I. W. Selesnick, "Bivariate shrinkage functions for wavelet-based denoising exploiting interscale dependency", *IEEE Trans. on Signal Processing*. 50(11): pp. 2744-2756, November 2002.

[15] N G Kingsbury, "A Dual-Tree Complex Wavelet Transform with improved orthogonality and symmetry properties", *Proc. IEEE Conf. on Image Processing*, Vancouver, September 11-13, 2000, paper 1429.

[16] G.P. Nason, "Choice of wavelet smoothness, primary resolution and threshold in wavelet shrinkage", *Statistics and Computing*, 12, pp. 219-227, 2002.

[17] H. Zhang, A. Nostratinia, R. O. Wells Jr., "Image Denoising via Wavelet-Domain Spatially Adaptive FIR Wiener Filtering", *IEEE ICASP*, vol. 5, 2179-2182, Istanbul, June 2000.

[18] D. L. Donoho, I. M. Johnstone, "Ideal spatial adaptation by wavelet shrinkage", *Biometrika*, 81(3) : 425-455, 1994.

[19] Hua Xie, Leland E. Pierce and Fawaz T. Ulaby, "Statistical Properties of Logarithmically Transformed Speckle", *IEEE Transactions on Geoscience and Remote Sensing*, vol. 40, no. 3, pp. 721-727, March 2002.

[20] J. Portilla, V. Strela, M. Wainwright and E. Simoncelli, "Adaptive Wiener Denoising Using Gaussian Scale Mixture Model", in *Proc. ICIP*, 2001.

[21] D. L. Donoho, "Denoising by soft-thresholding", *IEEE Trans. on Information Theory,* pp. 613-627, vol. 41, May, 1995.